TRENDS IN SCIENCES 2025; 22(9): 10384
https://doi.org/10.48048/tis.2025.10384
RESEARCH ARTICLE

DFT Analysis on Electronic Properties, Reactivity and Adsorption Mechanism of Favipiravir/$XTiO_4H_2$ (X = Pt, Zr, Zn) Nanocomplexes and their Biological Evaluations

Kamal Khanal, Mohan Bahadur Kshetri, Madan Khanal, Arjun Acharya, Rajesh Maharjan, Kalpana Gyawali, Madhav Prasad Ghimire and Tika Ram Lamichhane*

Central Department of Physics, Tribhuvan University, Kirtipur, Kathmandu, Nepal

(*Corresponding author's e-mail: tika.lamichhane@cdp.tu.edu.np)

Received: 17 April 2025, Revised: 12 May 2025, Accepted: 25 May 2025, Published: 10 July 2025

Abstract

The objective of this study is to explore quantum chemical properties of favipiravir-loaded $XTiO_4H_2$ nanostructures (X = Pt, Zr, Zn) using density functional theory and to evaluate their toxicity profiling, drug-likeness and binding efficacy to the target proteins. Favipiravir interacted strongly with $XTiO_4H_2$ forming the stable nanocomplexes (NCs) having adsorption energy in the range of −2.49 to −4.70 eV in gas phase. The HOMO-LUMO energy gap of favipiravir was 3.56 eV whereas Fav + $PtTiO_4H_2$ (NC1), Fav + $ZrTiO_4H_2$ (NC2), and Fav + $ZnTiO_4H_2$ (NC3) exhibited lower energy gaps of 1.23, 1.43 and 0.65 eV in gas phase, respectively, showing better reactivity of these NCs. The results of dipole moment, global reactivity descriptor, MEP surface, NBO, QTAIM and NCI of the proposed NCs were more favorable than that of favipiravir. The functionalized TiO_2 NCs exhibited better docking scores, among which NC2 showed the strongest inhibition of SARS-CoV-2 main protease and spike protein. NC3 having the predicted LD50 of 3,000 mg/kg in toxicity class V appears to be less toxic than favipiravir having LD50 of 1,717 mg/kg in the class IV. This study confirms the possibility of using transition metal-doped titania nanostructures for targeted drug delivery, antiviral therapy and photocatalytic degradation of the drugs.

Keywords: Density functional theory, Favipiravir, TiO_2 nanocomplexes, Reactivity, Charge transfer, Protein-ligand interactions

Introduction

One of the antiviral drugs, favipiravir inhibits SARS-CoV-2 RNA replication [1]; however, its performance is limited. To improve functionality of the drug candidates, the structural modification can be performed by interacting with transition metal-doped titanium dioxide (TiO_2). The functionalized TiO_2 nanostructures are biocompatible and less toxic offering sustainable drug delivery and release. The modified TiO_2 could be efficient therapeutic agents against COVID-19 [2]. The TiO_2 nanostructures have demonstrated encouraging promise in a number of biological applications, including tissue engineering, photodynamic therapy, drug transport, antimicrobial activity, and biosensing [3]. They are used in drug delivery systems due to biocompatibility, functionalization ability, and potential as photosensitizers [4]. When exposed to UV-radiation, TiO_2 exhibits photocatalytic properties and generates active oxygen-containing radicals. Furthermore, the TiO_2 nanostructures act as powerful antimicrobial agents by generating reactive oxygen species (ROS), including hydroxyl radicals (OH) and hydrogen peroxide (H_2O_2), under visible light, causing oxidative stress that kills virus and bacteria [5]. Zr-doped TiO_2 demonstrates promising biological responses due to its excellent biocompatibility. The $ZrTiO_2$ anatase

nanostructures are influencing their physicochemical properties exhibiting photocatalytic and antimicrobial activity [6]. Using metal nanostructure in drug delivery systems can reduce side effects by directly targeting the affected organ, thereby minimizing unwanted effects [7].

When Pt is doped into TiO_2, the band gap is reduced, charge separation is made easier, and photosensitization is improved [8]. Gutierrez *et al.* [9] studied functionalized TiO_2 based nanostructures absorbed with flavonoids that target the spike glycoprotein to prevent SARS-CoV-2 entry and fusion. Mazurkova *et al.* [10] analyzed TiO_2 nanostructures degrading the lipid envelope of influenza virus and suggested for antiviral treatments and disinfection by careful evaluation of their impact on the cell membrane. Depending on the nanostructure concentration and incubation time, TiO_2 inactivated the influenza virus. Adsorption of the drug molecules on the active surfaces of transition metal-doped TiO_2 nanostructure holds immense potential for drug development in medical field [7]. TiO_2 nanostructures offer vary large surface area allows high drug carrying capacity and flexibility [11].

Density functional theory (DFT) is employed to predict the structural, molecular, and electronic properties of the nanocomplexes (NCs). The hybrid exchange-correlation functional B3LYP with LANL2DZ basis set has proven efficiency and reliability in analyzing conjugated systems and species containing lone pairs. TiO_2 has been proposed as a carrier in medical, biological or specific therapeutic applications due to its minimal toxicity and superior biocompatibility [12]. The adsorption of drug molecules on TiO_2 alters its band gap, acting like dopants and enhancing the material's sensitivity to the electromagnetic spectrum [13]. Evaluating ADME parameters alongside toxicity is essential for identifying safe and effective drug candidates during the drug development [14]. This research focuses on the structural modification and quantum chemical study of favipiravir by interacting with Pt/Zr/Zn-TiO_2 nanostructures using DFT, the binding affinity or inhibition potential against SARS-CoV-2 Mpro and spike protein using molecular docking, and the evaluation of their drug-likeness and toxicity using ADMET analysis.

Materials and methods

DFT study on nanocomplexes

The structure of favipiravir (CID 492405) was obtained from the PubChem database. Pt/Zr/Zn-TiO_4H_2 nonostructures were prepared by modifying crystal structure of anatase TiO_2 retrieved from PubChem in cif format using Gaussian 16 software [15] as described in Ikram *et al.* [6] and Kumar *et al.* [8]. 2 dimensional and 3 dimensional views of $ZrTiO_4H_2$ nanostructure have been shown in **Figures S1 (a) and (b)**. Quantum chemical properties of favipiravir and its composition with Pt/Zr/Zn-TiO_4H_2 were optimized by using the DFT method in B3LYP [16,17] level of theory with LANL2DZ basis set [18] GaussView 6.0 [19] was used to perform nanocomplex visualization and GaussSum 3.0 software was used to produce density of states (DOS) spectrum [20]. Natural bond orbital (NBO) analysis was performed using NBO 3.0 [21] program in the same level of DFT. The topological surfaces were analyzed using Multiwfn software [22].

Molecular docking

The crystal structure of SARS-CoV-2 Mpro (PDB ID: 6LU7, resolution 2.16 Å) [23] and spike-ACE2 protein (PDB ID: 6MOJ, resolution 2.45 Å) [24] were downloaded from the RCSB Protein Data Bank [25-27] and refined using online server SWISS-MODEL [28]. Molecular docking was performed by using AutoDock 4.2.6 tools [29]. Proteins and ligands were prepared by eliminating water molecules, adding Kollmann's charges, incorporating polar hydrogens, ensuring the ligands with zero rotatable bonds. A grid box having size 80 Å × 80 Å × 80 Å, central grid points (−8.368 Å, −38.315 Å, and −16.429 Å) and grid point spacing 0.375 Å was used. Using the Lamarckian Genetic Algorithm with population size 150 and energy evaluations 2,500,000, 10 runs were conducted to generate docking parameter files. The best-docked conformer was subjected to BIOVIA Discovery Studio Visualizer [30] to analyze hydrogen bonding, van der Waals, hydrophobic and electrostatic interactions between ligand and protein. By *in silico* techniques including molecular docking, the inhibition potential of the drug candidates against different target proteins have been explained in the recent researches [31,32].

ADMET calculations

The physicochemical, drug-likeness, lipophilicity, and water solubility of favipiravir/$XTiO_4H_2$ NCs were studied using SwissADME webserver [33] and toxicity using ProTox-II [34]. Also, topological polar surface area (TPSA) and Lipinski's rule of five (Ro5) [14] of the proposed structures were analyzed.

Results and discussion

Geometrical parameters

Geometrical optimization finds the atomic arrangement in a stable molecule corresponding to the lowest energy state [35]. The geometry parameters of the optimized nanocomplex in gas phase and water solvent are identified using the DFT method at B3LYP/LANL2DZ level of calculations. Favipiravir undergoes separate adsorption with $Ti_2O_4H_2$, $PtTiO_4H_2$, $ZrTiO_4H_2$, and $ZnTiO_4H_2$, resulting in the formation of Fav+$Ti_2O_4H_2$, Fav+$PtTiO_4H_2$ (NC1), Fav+$ZrTiO_4H_2$ (NC2), and Fav+$ZnTiO_4H_2$ (NC3) nanocomplexes. The geometrical parameters of favipiravir remain nearly unchanged while forming the NCs which are shown in supplementary **Tables S1, S2 and S3**. The optimized Fav+$Ti_2O_4H_2$ nanocomplex structure in gas phase and water solvent is shown in **Figures S1** (**c**) **and** (**d**). The optimized nanocomplex Pt/Zr/Zn-doped $Ti_2O_4H_2$ structures are shown in **Figure 1** in the gas phase and supplementary **Figure S2** in the water solvent. The dipole moments in the gas phase and water solvent can have an impact on the distribution of charges across the structures of the system through the dipole-dipole interactions forming the intermolecular hydrogen bonds [36]. The dipole moments of favipiravir, Fav+$Ti_2O_4H_2$, NC1, NC2, and NC3 are found to be 5.70, 4.12, 12.14, 5.31 and 16.07 Debye in the gas phase whereas 8.35, 6.88, 24.00, 13.69 and 28.23 Debye in the water solvent, respectively. Here, Fav+$Ti_2O_4H_2$ has the lowest dipole moment. The highest dipole moment of NC3 suggests that it strongly participates in the polar reactions [37].

Adsorption energy

The value of adsorption energy measurement signifies the strength of interactions between adsorbate and adsorbent. The adsorption energy (E_{ads}) is computed using Equation 1 [35].

$$E_{\text{ads}} = E_{\text{Fav+XTiO}_4\text{H}_2} - E_{\text{XTiO}_4\text{H}_2} - E_{\text{Fav}} \quad (1)$$

The most stable conformer of Fav/$XTiO_4H_2$ nanocomplex has been identified by its geometry optimization on which the C=O groups of favipiravir bind strongly with $XTiO_4H_2$ (**Figure 1**). The adsorption energy of favipiravir molecule with the pristine titania nanostructure ($Ti_2O_4H_2$) is −4.65 eV in gas phase and −3.23 eV in water solvent. While the favipiravir molecule interacts with Pt/Zr/Zn-doped titania, the highest negative interaction energy is seen in the NC2 nanocomplex, with a value of −4.70 eV in gas phase and −3.78 eV in water solvent (**Table S4**). Therefore, NC2 preserves the strongest interactions recommending chemisorption between favipiravir and Zr-doped titania nanostructure. The negative adsorption energy shows that each of the proposed NCs is stable in both phases.

Frontier molecular orbitals

The molecule with smaller HOMO-LUMO energy gap exhibits higher reactivity, higher polarizability, and lower kinetic stability [38]. In **Figure 2,** the red region surrounding the atoms indicates the positive phase, while the green region indicates the negative phase [39]. For favipiravir, NC1, NC2 and NC3, the HOMO-LUMO energy gaps are observed to be 3.56, 1.23, 1.43 and 0.65 eV in gas phase (**Figure 2**) and 3.86, 2.31, 1.87 and 2.81 eV in water solvent (**Figure S3**), respectively. The computed values are consistent with those determined by the DOS spectra as in **Figure 3** in gas phase and in water solvent (**Figure S4**). In the gas phase, the NC3 nanocomplex is softer and more reactive than the other nanocomplexes due to the narrow energy gap that makes electron transport easier. However, in the water solvent, the NC2 nanocomplex appears to be more reactive.

Global reactivity descriptors

Global reactivity descriptors help to describe the electronic structure and predict its reactivity [40]. The energies of frontier orbitals indicate the ionization potential of the molecules and electron affinity means the electron-donating and accepting nature. The global

reactivity descriptors such as HOMO-LUMO energy gap, electron affinity (EA), electronegativity (χ), ionization potential (IP), chemical potential (μ), chemical softness (S), chemical hardness (η), and electrophilicity index (ω) [41]. Their values obtained for the proposed nanocomplexes are depicted in **Table 1.**

The HOMO-LUMO energy gap of favipiravir is identified as 3.56 eV in gas and 3.86 eV in water solvent which are matching with the previously reported values [42]. After interacting favipiravir with the pristine $Ti_2O_4H_2$ nanostructure, the HOMO-LUMO energy gap is reduced to 1.32 eV in gas phase and 1.39 eV in water solvent. The energy gap for NC1, NC2 and NC3 nanocomplexes are identified as 1.23, 1.43 and 0.65 eV in gas phase and 2.31, 1.87 and 2.81 eV in the water solvent, respectively. The lower energy gap suggests greater ease of intra-molecular charge transfer and more reactive nature of the molecules [43]. In the gas phase, NC3 offers the lowest value of hardness (0.32 eV) and the highest value of softness (1.53 $(eV)^{-1}$) showing its reactive nature. The electrophilicity index for favipiravir is 7.36 eV and for NC3 is 40 eV in gas phase. The larger electrophilicity index indicates improved bioavailability or greater ability to attract electrons [44]. In other words, the smaller values of electrophilicity index and chemical potential indicate nucleophilic nature and the larger values indicate electrophilic nature of the molecules [45].

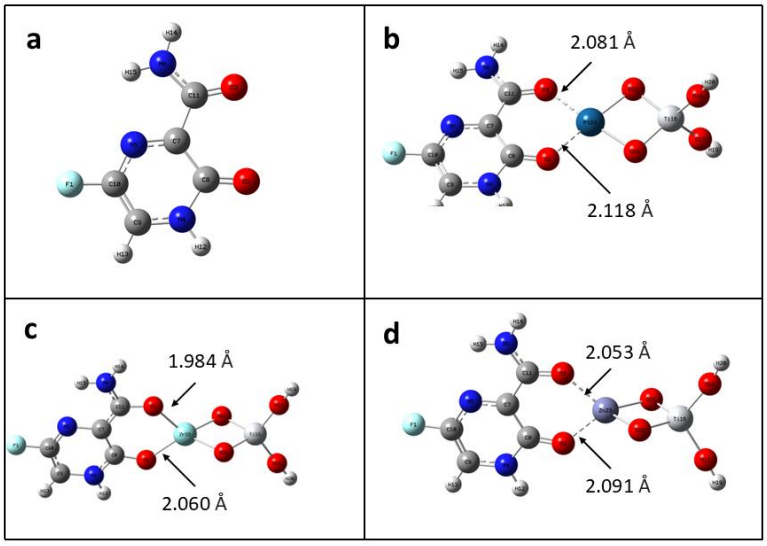

Figure 1 Optimized structure of (a) favipiravir, (b) Fav+$PtTiO_4H_2$, (c) Fav+$ZrTiO_4H_2$, and (d) Fav+$ZnTiO_4H_2$ nanocomplexes in gas phase.

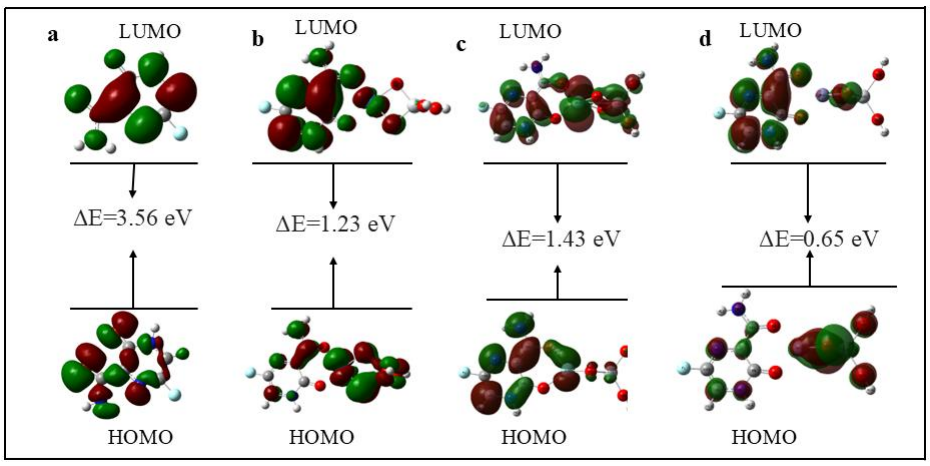

Figure 2 HOMO and LUMO energy gap of (a) favipiravir, (b) Fav+$PtTiO_4H_2$, (c) Fav+$ZrTiO_4H_2$, and (d) Fav+$ZnTiO_4H_2$ nanocomplexes in gas phase.

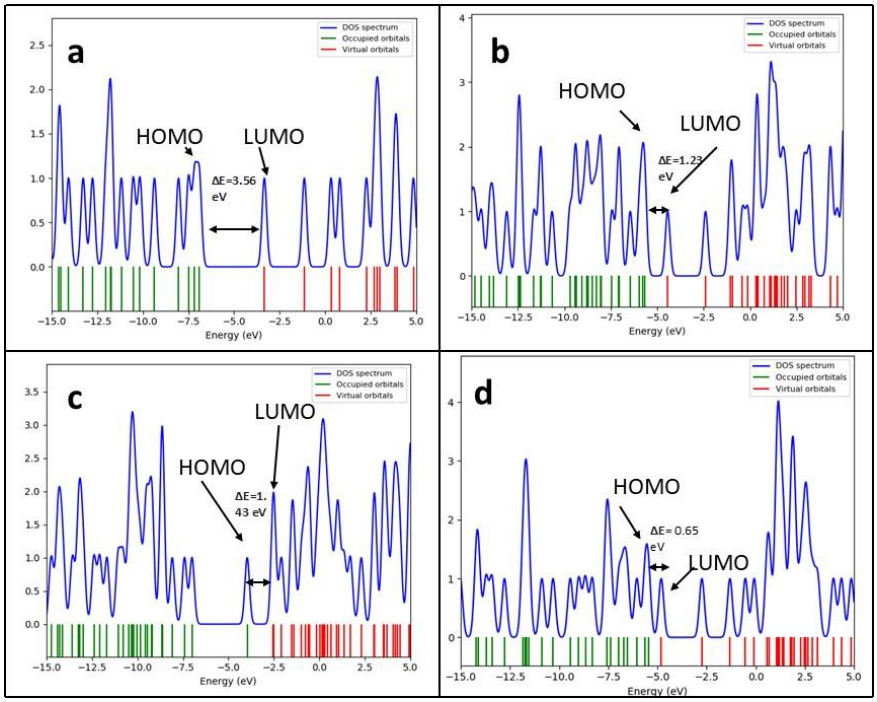

Figure 3 Density of states of (a) favipiravir, (b) Fav+$PtTiO_4H_2$, (c) Fav+$ZrTiO_4H_2$, and (d) Fav+$ZnTiO_4H_2$ nanocomplexes in gas phase.

Table 1 Chemical and electrochemical properties of favipiravir and Fav+Pt/Zr/Zn-TiO_4H_2 at gas phase and water solvent using B3LYP/LANL2DZ basis set.

Parameter	Favipiravir		Fav+$PtTiO_4H_2$ (NC1)		Fav+$ZrTiO_4H_2$ (NC2)		Fav+$ZnTiO_4H_2$ (NC3)	
	Gas	**Water**	**Gas**	**Water**	**Gas**	**Water**	**Gas**	**Water**
HOMO (E_{HOMO})(eV)	−6.90	−7.02	−6.90	−6.21	−3.97	−3.67	−5.46	−6.63
LUMO (E_{LUMO})(eV)	−3.34	−3.16	−4.44	−3.90	−2.54	−1.80	−4.81	−3.82
Ionization potential (IP) (eV)	6.90	7.02	5.67	6.21	3.97	3.67	5.46	6.63
Electron affinity (EA) (eV)	3.34	3.16	4.44	3.90	2.54	1.80	4.81	3.82
Energy gap (eV)	3.56	3.86	1.23	2.31	1.43	1.87	0.65	2.81
Electronegativity (χ) (eV)	5.12	5.09	5.06	5.05	3.26	2.74	5.14	5.22
Chemical potential (μ) (eV)	−5.12	−5.09	−5.06	−5.05	−3.26	−2.74	−5.14	−5.22
Hardness(η) (eV)	1.78	1.93	0.62	1.15	0.715	0.94	0.32	1.40
Softness(S) $(eV)^{-1}$	0.28	0.26	0.81	0.43	0.70	0.53	1.53	0.36
Electrophilicity index(ω) (eV)	7.36	6.74	20.77	10.96	7.41	3.97	40	9.81

Molecular electrostatic potential surface

Molecular electrostatic potential (MEP) surface provides a visualization of electronic and nuclear charge distribution across a molecule. In computational chemistry, MEP is used to identify nucleophilic and electrophilic regions within a molecule, evaluate its reactivity, and analyze its intermolecular interactions [46]. In MEP, the blue regions indicate most electropositive potential that correspond to the repulsion of a proton by the atomic nuclei. In contrast, the red regions representing most electronegative potential are associated with the attraction of a proton by the overall electron

density within the molecule, and green region indicates zero potential [47]. Here, NC3 nanocomplex has the higher potential regions ranging from −0.114 a.u. to 0.114 a.u. in comparison to the other nanocomplexes. The maximum positive regions are located on hydrogen (H12, H13) atoms for favipiravir, (H12, H13, H14, H15) atoms for NC1, (H12, H19, H20) atoms for NC2, and (H12, H13, H14, H15) atoms for NC3 nanocomplexes indicating possible sites for electrophilicity. The oxygen atoms (O2, O3) in favipiravir, (O21, O22) in NC1, NC2 and NC3 nanocomplexes have maximum negative charges, indicating the nucleophilic sites in gas phase as in **Figure 4** and in water solvent as shown in **Figure S5**.

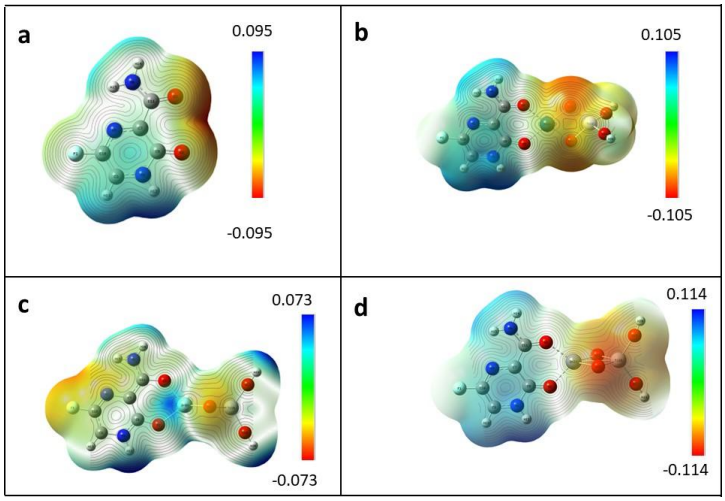

Figure 4 Molecular electrostatic potential diagrams for (a) favipiravir, (b) Fav + $PtTiO_4H_2$, (c) Fav + $ZrTiO_4H_2$, and (d) Fav + $ZnTiO_4H_2$ nanocomplexes in gas phase.

Mulliken and natural charges

Mulliken and natural charge calculations are essential for evaluating an electronic structure, molecular polarizability, and dipole moment in quantum chemical calculation [37]. The proposed nanocomplexes consist of negative charges on oxygen atoms and positive charges on hydrogen atoms whereas carbon atoms exhibit either positive or negative charges. The higher positive Mulliken and natural charges are detected in Ti, Pt, Zr, Zn and the higher negative charges are observed in O2, O3, N4, N6, O17, O18, O21 and O22. This type of distribution of charges is favorable for the formation of hydrogen bonds. Since Ti, Pt, Zr and Zn have the highest positive charges, they are attacked by nucleophiles. The oxygen atoms O17 and O18 are attacked by electrophiles because they have the highest negative charges as shown in supplementary **Tables S5, S6** and **Figures S6, S7** in gas phase and water solvent.

Thermodynamic properties

Thermodynamic properties are responsible for maintaining the thermal stability of a molecular system. The thermodynamic parameters such as enthalpy (ΔH), thermal energy (ΔE), Gibbs free energy (ΔG), specific heat capacity (C_v), and entropy (S) have been calculated for favipiravir and nanocomplexes at room temperature (298.15 K) which are depicted in supplementary **Table S7**. The negative value of ΔG indicates that favipiravir interacts spontaneously with the TiO_2 nanostructures and the interaction is thermodynamically favorable. Furthermore, these thermodynamic properties of the nanocomplexes are also favorable to strong interactions with the target proteins [48]. The parameters ΔE, C_v and S have been calculated by optimizing nanocomplexes in the 50 - 500 K temperature range as presented in the supplementary **Tables S8, S9, S10 and S11**. As shown in **Figures S8, S9, S10 and S11**, ΔE, C_v and S exhibit an increasing trend with temperature, which is due to the increase in the vibrational intensities of molecules [49]. The correlation graphs from the best-fitted analysis obtain the empirical relations supported by the coefficient of determination nearly one.

Ultraviolet-visible absorption analysis

The ultraviolet-visible (UV-Vis) spectra are

explained charge transfer, absorption properties, and excitation energies of favipiravir, NC1, NC2 and NC3 nanocomplexes. The maximum absorption wavelength and the oscillator strength in the gas phase and water solvent are depicted in **Table S12**. For favipiravir, the primary absorption peak in the UV-Vis region is observed at a wavelength of 343 nm in the gas phase and 356 nm in the water solvent. In comparison, the NC1 exhibits a higher absorption peak at a wavelength of 1,981 nm in the gas phase and 690 nm in the water solvent. NC2 shows a higher absorption peak at 933 nm in the gas phase and 773 nm in the water solvent. For NC3, the absorption peak appears at 2,244 nm in the gas phase and 532 nm in the water solvent. When favipiravir is combined with $XTiO_4H_2$ nanostructures, there is a red-shift in the absorption of ultraviolet light, with the most substantial shift seen in NC3 nanocomplex (see **Figures S12 and S13**). The protective film of nanomedicine blocks or absorbs both UV and red light [50], ensuring their maximum potency in gas phase as well as water solvent.

Local reactivity descriptors

The Fukui function is commonly used to analyze the charge distribution, focusing on local reactivity parameters that explain chemical activity and identify specific reactive sites of a molecule. It predicts the locations within the molecule that are susceptible to nucleophilic, electrophilic, and radial attacks [51]. The difference between electrophilic and nucleophilic Fukui functions is known as dual descriptor given by Equation 2 [52-54].

$$\Delta f(r) = [f_k^+(r) - f_k^-(r)] \quad (2)$$

The nucleophilic attack is preferred if $\Delta f(r) > 0$ whereas the electrophilic attack is preferred if $\Delta f(r) < 0$. In favipiravir, NC1, NC2, and NC3, the nucleophilic attacks are found in the sites (N4, N6), (O22, Pt23), (N6, C11) and (O21, O22) whereas electrophilic attacks are found in the sites (C8, C11), (C7, C9), (Ti16, Zr23) and (C7, C9), respectively. The related values of the dual descriptors are mentioned in the supplementary **Tables S13, S14, S15 and S16.**

Natural bond orbital (NBO) analysis

The NBO analysis is useful to understand intramolecular bonding and charge transfer mechanism in a molecular system [55]. The NBO analysis investigates molecular stability, focusing on the charge transfer and hyper-conjugative interactions within the structure. The interaction between the donor and acceptor orbitals becomes stronger as the stabilization energy $E(2)$ increases [56]. The energy $E(2)$ related to the donor and acceptor orbitals is calculated by using the theory of second-order perturbation as mentioned in Equation 3 [57,58].

$$E(2) = q_i \frac{F^2(i,j)}{E_j - E_i} \quad (3)$$

where q_i represents the occupancy of the donor orbitals, E_i and E_j are the diagonal elements, and $F(i,j)$ is the off-diagonal elements of the Fock matrix or Kohn-Sham matrix corresponding to the energies of the donor and acceptor orbitals.

The interaction from nonbonding donor orbitals, i.e. lone pair of electrons LP(1)N6 to antibonding π^*(O3-C11) orbital leads to the highest stabilization energy of 67.25 kcal/mol for favipiravir. Again, LP(1)N4 to π^*(O2-C8), and LP(1)N4 to π^*(C9-C10) have stabilization energies of 43.73 kcal/mol, and 43.43 kcal/mol, respectively. The interaction from nonbonding donor orbitals LP(2)N5 to antibonding LP*(1)C7 orbital leads to the highest stabilization of 380.16 kcal/mol for NC1. In the same nanostructure, LP(1)C10 to π^*(N4-C9), and LP(1)N6 to π^*(O3-C11) have stabilization energies of 233.60 kcal/mol, and 81.31 kcal/mol, respectively. For NC2 structure, LP(1)C7 to π^*(O2-C8) leads to the highest stabilization of 599.80 kcal/mol. Again, LP(1)C7 to π^*(N6-C11), and LP(1)O22 to LP*(2)Zr23 have stabilization energies of 304.29 kcal/mol, and 42.16 kcal/mol, respectively. In this way, for NC3, LP(2)N5 to LP*(1)C7 provide the significant stabilization of 384.30 kcal/mol. In this structure, LP(1)C10 to π^*(N4-C9), and LP(1)N6 to π^*(O3-C11) have stabilization energies of 224.90 kcal/mol and 86.98 kcal/mol, respectively. Comparing the NBO results among the proposed nanocomplexes, NC2 offers the highest stabilization energy. The related NBO results are depicted in the supplementary **Tables S17, S18, S19 and S20**.

Non-covalent interaction (NCI) analysis

The NCI describes the local bonding properties

including electron density (ρ) and reduced density gradient (RDG). RDG approach is a useful topological method based on electron density and its derivatives [59]. The combination of RDG and ρ enables a basic division in bonding regions. The high RDG and low ρ indicate non-interacting density tails, low RDG and high ρ correspond to covalent bonds, whereas low RDG and low ρ are related to non-covalent interactions. The NCIs are weak in comparison to covalent bonding. Both RDG and ρ having low values isolate weak interactions. The interaction strength is evaluated by examining the graph plotted for sign(λ_2)ρ *vs.* RDG, where λ_2 represents second eigenvalue of the electron density Hessian matrix. Here, $\lambda_2 = 0$, $\lambda_2 < 0$, and $\lambda_2 > 0$ refer to weak van der Waals, strong H-bonding, and repulsive steric effects represented by green, blue and red regions, respectively [60]. The RDG plots shown in **Figure 5** describe the nature of interactions between favipiravir and $ZnTiO_4H_2$ nanostructures. The blue RDG graph between the sign(λ_2)ρ values −0.02 and −0.05 a.u. demonstrates the additional strong hydrogen bonding. The existence of potent intramolecular hydrogen bonding in the molecules plays a crucial role for biological activity [61]. The 3 dimensional isosurface densities and 2 dimensional scatter plots of favipiravir and the proposed NCs are shown in **Figures S14 and S15.**

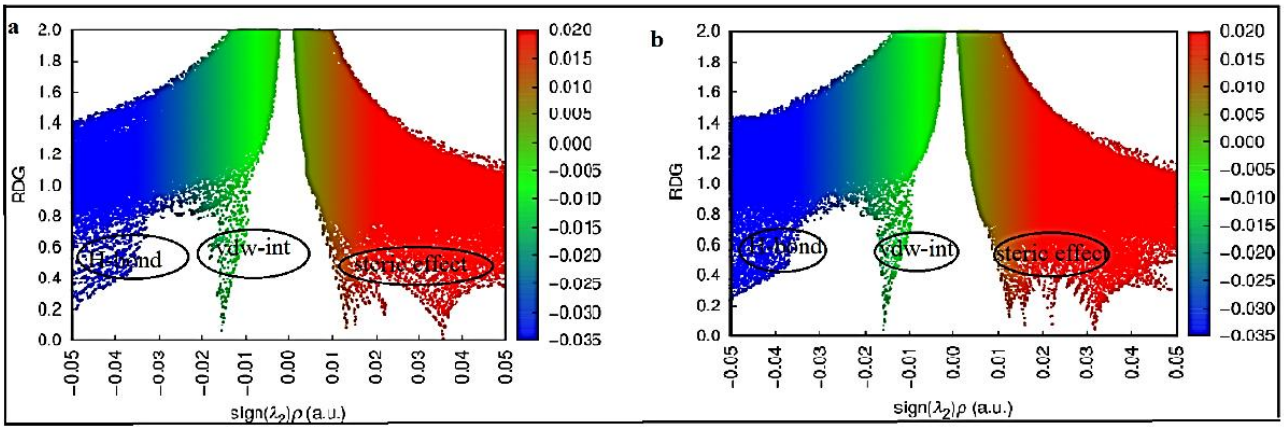

Figure 5 Reduced density gradient (RDG) scatter graph for Fav+$ZnTiO_4H_2$ nanocomplex in (a) gas phase and (b) water solvent showing H-bonding, van der Waals (vdW), and steric interactions.

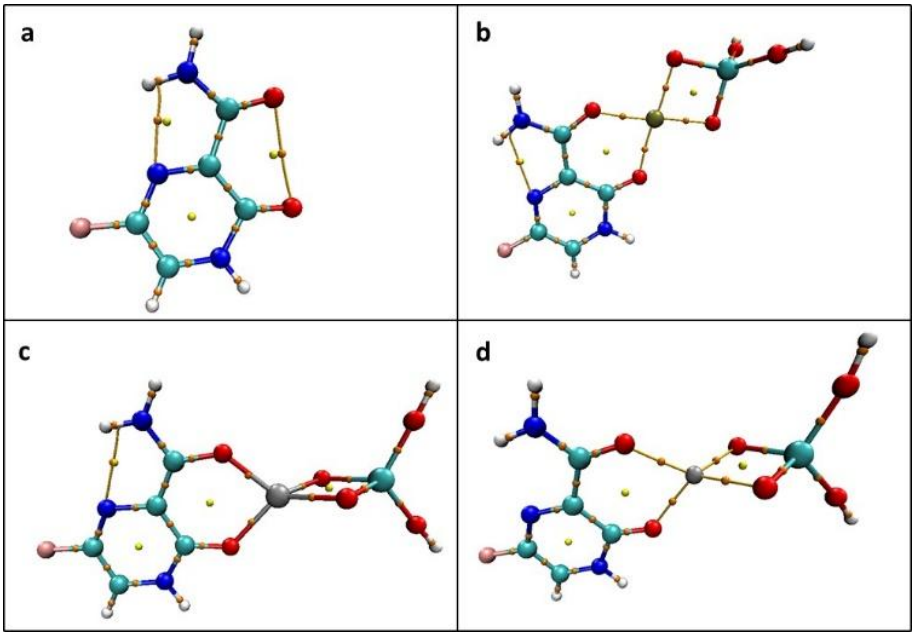

Figure 6 QTAIM diagram of (a) favipiravir, (b) Fav+$PtTiO_4H_2$, (c) Fav+$ZrTiO_4H_2$, and (d) Fav+$ZnTiO_4H_2$ nanocomplexes in gas phase.

Quantum theory of atoms in molecules (QTAIM) analysis

The QTAIM is a potent method for estimating inter molecular interactions by using topological characteristics to determine the bond critical point (BCP) between interacting systems. In BCPs, the computed values of electron density (ρ) range from 0.0534 to 0.1125 a.u. and that of $\nabla^2\rho$ range from 0.2963 to 0.5425 a.u for the proposed NCs. From **Table 2**, it has been observed that the value of ρ is raised when Zr is replaced with Pt and Zn in the TiO_2 nanostructures. The electron density features of the NCs imply positive $\nabla^2\rho$ and high charge densities of X-O bonds where X refers to Pt, Zr and Zn. Here, H(r) < 0 so that interaction has a dominant covalent character due to the potential energy contribution stronger than the kinetic energy. The positive values of $\nabla^2\rho$ and negative H(r) for intra- and intermolecular hydrogen bonding indicate the partly covalent nature. Therefore, the X-O bonds in the NCs have a mix of ionic and covalent bonding [62]. The QTAIM results are consistent with the interaction trends projected in adsorption energy and NBO analysis referring NC2 as the potent drug candidate. QTAIM diagrams of NCs as shown in **Figure 6**.

Table 2 The electron density (ρ), Laplacian of electron density $\nabla^2\rho$, Lagrangain kinetic energy (G(r)), kinetic energy density K(r)), potential energy density (V(r)), total electron energy density (H(r)) in a.u. at BCPs in the favipiravir absorbed with nanocomplexes by AIM analysis in gas phase.

Complexes	BCP	ρ	$\nabla^2\rho$	G(r)	K(r)	V(r)	H(r)	K(r)/V(r)|
Fav+$PtTiO_4H_2$ (NC1)	O2-Pt23	0.0782	0.4589	0.1228	0.0097	−0.1325	−0.0097	0.0731
	O3-Pt23	0.0850	0.5034	0.1356	0.0117	−0.1474	−0.0117	0.0795
Fav+$ZrTiO_4H_2$ (NC2)	O2-Zr23	0.0940	0.4599	0.1273	0.0125	−0.1398	−0.0125	0.0874
	O3-Zr23	0.1125	0.5425	0.1586	0.0234	−0.1820	−0.0234	0.1287
Fav+$ZnTiO_4H_2$ (NC3)	O2-Zn23	0.0534	0.2963	0.0678	0.0079	−0.0758	−0.0079	0.1047
	O3-Zn23	0.0582	0.3385	0.0760	0.0083	−0.0844	−0.0083	0.0989

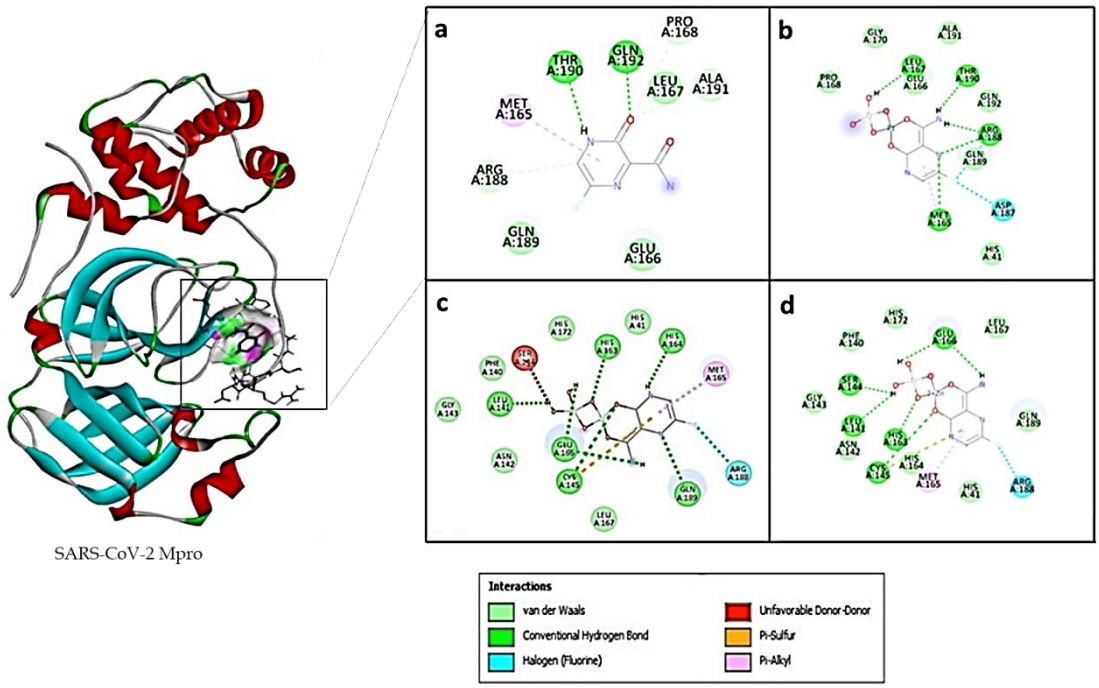

Figure 7 Interactions of (a) favipiravir, (b) Fav+$PtTiO_4H_2$, (c) Fav+$ZrTiO_4H_2$, and (d) Fav+$ZnTiO_4H_2$ nanocomplexes with active amino acid residues of SARS-CoV-2 Mpro for molecular docking.

Molecular docking analysis

The key residues in the receptor site of Mpro include Met49, Phe140, Asn142, Gly143, Cys145, His163, His164, Met165, Glu166, leu167, Pro168, His172, Gln189, Ala191 and Gln192 [23]. In the receptor site of spike-ACE2, the residues Lys417, Gly446, Tyr449, Tyr453, Phe456, Ala475, Phe486, Asn487, Tyr489, Gln493, Gly496, Gln498, Thr500, Asn501, Gly502 and Tyr505 actively participate in protein-ligand interactions [63]. The docking scores of favipiravir with Mpro and spike protein are −3.99 and −4.77 kcal/mol having inhibition constants of 1,190 μM and 321.06 μM, respectively.

In the Mpro-favipiravir complex, 2 hydrogen bonds are formed between favipiravir and residues Thr190 and Gln192 at distances of 2.03 and 2.05 Å. Hydrophobic interactions involve Glu166, Leu167 and Gln189 while carbon hydrogen bonds are formed with Pro168, Arg188 and Ala191. Met165 participates in π-alkyl interactions. For the spike protein, favipiravir forms 4 H-bonds with Tyr279, Pro289, Ile291 and Asn437 at distances of 1.95 Å, 1.95 Å, 2.22 Å and 2.30 Å, respectively. It also forms hydrophobic interactions with residues Lys288, Met366, Phe428, Thr434, Phe438 and Lys441. Asn290 is involved in halogen interaction in the spike protein.

Table 3 Molecular docking results of favipiravir, Fav+$PtTiO_4H_2$, Fav+$ZrTiO_4H_2$, and Fav+$ZnTiO_4H_2$ nanocomplexes with Mpro and spike-ACE2 protein.

Parameter	Favipiravir		Fav+$PtTiO_4H_2$ (NC1)		Fav+$ZrTiO_4H_2$ (NC2)		Fav+$ZnTiO_4H_2$ (NC3)	
	Mpro	**Spike**	**Mpro**	**Spike**	**Mpro**	**Spike**	**Mpro**	**Spike**
Final intermolecular energy (kcal/mol)	−4.29	−5.06	−5.49	−5.71	−6.01	−6.45	−6.14	−6.62
Inhibition constant (μM)	1190	321.06	93.87	62.28	62.11	29.63	202.64	89.74
Estimated free energy of binding (kcal/mol)	−3.99	−4.77	−5.49	−5.74	−5.74	−6.18	−5.04	−5.52

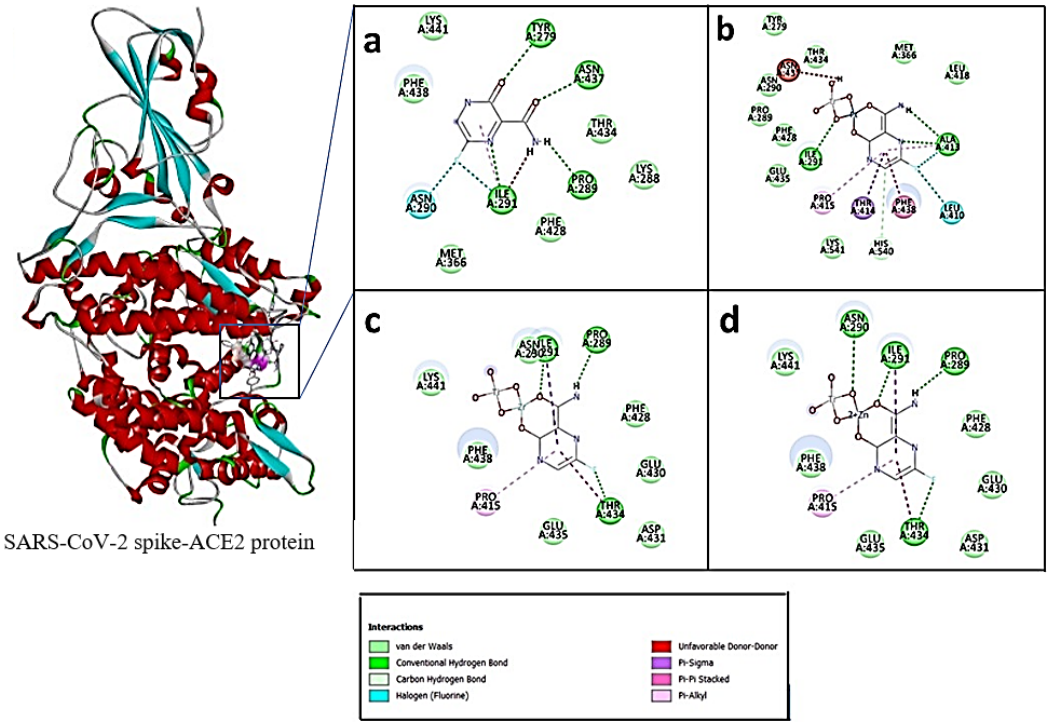

Figure 8 Interactions of (a) favipiravir, (b) Fav+$PtTiO_4H_2$, (c) Fav+$ZrTiO_4H_2$, and (d) Fav+$ZnTiO_4H_2$ nanocomplexes with active amino acid residues of SARS-CoV-2 spike-ACE2 by molecular docking.

The docking score of NC2 with Mpro and spike are −5.74 and −6.18 kcal/mol resulting in the inhibition constant of 62.11 and 29.63 μM, respectively. It is seen that the NC2 forms 5 H-bonds with Mpro residues Leu141, Cys145, His163, His164 and Glu166 at distance of 1.84, 3.59, 2.36, 2.91 and 1.75 Å; hydrobhobic interactions with His41, Phe140, Asn142, Gly143, Met165, Leu167, His172 and Gln189; halogen bond with Arg188; and unfavorable donor-donor interaction with Ser144. In this way, NC2 forms 3 H-bonds with spike Pro289, Ile291 and Thr434 at distance of 1.78 Å, 1.84 Å and 2.47 Å, respectively. Hydrobhobic interactions involve Asn290, Phe428, Glu430, Asp431, Glu435, Phe438 and Lys441; π-alkyl includes Pro415. Various interactions of favipiravir, NC1, NC2 and NC3 nanocomplexes with Mpro and spike protein are illustrated in **Figure 7** and **Figure 8**. The values of intermolecular energy, binding energy, and inhibition constant are summarized in **Table 3.** The binding energy, interacting amino acid residues and H-bonds formation collectively indicate that NC2 exhibits the highest binding efficacy with SARS-CoV-2 Mpro and spike protein. The active amino acid residues and the nature of H-bonds have been presented in supplementary **Tables S21 and S22**.

ADMET analysis

Drug-likeness describes the potential of a drug molecule as an oral medication, mostly based on its bioavailability. The suitable drug candidates efficiently enter the body, attach to target proteins, and have therapeutic effects. According to Lipinski's Ro5, the oral drugs should have molecular mass (≤ 500 Daltons), hydrogen bond donors (≤ 5), hydrogen bond acceptors (≤10) and octanol-water partition coefficient (≤ 5) [14]. Using *in silico* techniques, the potential antiviral and anticancer drug candidates that follow Lipinski's RO5 have been analyzed in the recent researches [64, 65]. The proposed NCs also closely follow the Lipinski's Ro5. The bioavailability radar diagram evaluates six physicochemical characteristics including lipophilicity, size, polarity, solubility, saturation, and flexibility. The NCs cover the pink region, indicating drug-likeness as in **Figure S16**. The estimated water solubility values for favipiravir, NC1, NC2 and NC3 are −0.80, −1.5, −0.70, and −0.70, respectively. Furthermore, TPSA values are 88.8, 127.5, 127.9 and 127.5 $Å^2$ (below 140 $Å^2$) and synthetic accessibility scores are 2.08, 4.83, 5.15 and 5.03 for favipiravir, NC1, NC2 and NC3, respectively. The bioavailability score for all NCs is 0.6 which indicates their favorable pharmacokinetic properties. The computed values of ADME parameters for favipiravir, NC1, NC2 and NC3 nanocomplexes have been listed in **Table S23**.

Toxicity is commonly expressed through LD50 values (mg/kg body weight) along with corresponding toxicity classes predicted using ProTox II webserver. Their corresponding LD50 values and other toxicity are the 5 analyses used to predict hepatotoxicity, carcinogenicity, immunotoxicity, mutagenicity, and cytotoxicity [66]. Favipiravir has the predicted LD50 of 1,717 mg/kg in toxicity class IV. NC3 has the predicted LD50 of 3,000 mg/kg in the toxicity class V with reduced toxicity. The LD50 values and the toxicity classes of favipiravir, NC1, NC2 and NC3 nanocomplexes are listed in **Table S24**. The results show that the proposed NCs may be effectively transported into the human lipid system. The NCs could be the potential drug candidates, but further research must be necessary.

Conclusions

Favipiravir-loaded transition metal-doped titania (Fav/$XTiO_4H_2$, X = Pt, Zr, Zn) appeared stable nanocomplexes (NCs) with high adsorption energy and low HOMO-LUMO energy gap. With the lowest HOMO-LUMO energy gap, Fav+$ZnTiO_4H_2$ nanocomplex was more reactive than the other two NCs. Furthermore, Fav+$ZnTiO_4H_2$ offered more favorable pharmacokinetic properties and lower toxicity. The strong binding affinities of the proposed NCs with Mpro and spike protein, reflected in docking scores and inhibition constants, suggested their promising potential against SARS-CoV-2. The Fav+$ZrTiO_4H_2$ nanocomplex demonstrated better binding efficacy than the other two NCs. These findings are in support of the functionalized TiO_2 NCs exhibiting antimicrobial activity with the reduced toxicity.

Acknowledgments

We acknowledge Prof. Dr. Rajendra Parajuli and Asst. Prof. Pitambar Shrestha of Amrit Science College, Tribhuvan University, Kathmandu, Nepal for providing access to Gaussian calculations. We thank Prof. Dr. Hari Prasad Lamichhane for the technical support. We are grateful to University Grants Commission (UGC) Nepal for providing Small RDI Grant (Award No. SRDIG-81/82-S&T-01) in support to this research.

Declaration of Generative AI in Scientific Writing

The authors declare that no generative AI tool has been used in data generation, interpretation, and preparation of this manuscript. The authors take full responsibility for the content and conclusions of this work.

CRediT Author Statement

Kamal Khanal: Study design, data analysis, manuscript writing.

Mohan Bahadur Kshetri: Critical feedback and revised the manuscript.

Madan Khanal: Critical feedback, data analysis and revised the manuscript.

Arjun Acharya: Critical feedback and revised the manuscript.

Rajesh Maharjan: Critical feedback and revised the manuscript.

Madhav Prasad Ghimire: Review and editing.

Tika Ram Lamichhane: Manuscript revision, technical support and supervision.

References

[1] S Ludwig and A Zarbock. Coronaviruses and SARS-CoV-2: A brief overview. *Anesthesia & Analgesia* 2020; **131(1)**, 93-96.

[2] FH Haghighi, M Mercurio, S Cerra, TA Salamone, R Bianymotlagh, C Palocci, VR Spica and I Fratoddi. Surface modification of TiO_2 nanoparticles with organic molecules and their biological applications. *Journal of Materials Chemistry B* 2023; **11**, 2334-2366.

[3] A Ul-Hamid, N Baig, A Haider, AS Hakeem and M Ikram. Using biologically synthesized TiO_2 nanoparticles as potential remedy against multiple drug resistant Staphylococcus aureus of bovine mastitis. *Scientific Reports* 2023; **13**, 18785.

[4] S Chibber and I Ahmad. Molecular docking, a tool to determine interaction of CuO and TiO_2 nanoparticles with human serum albumin. *Biochemistry and Biophysics Reports* 2016; **6**, 63-67.

[5] M Cho, H Chung, W Choi and J Yoon. Different inactivation behaviors of MS-2 phage and Escherichia coli in TiO_2 photocatalytic disinfection. *Applied and Environmental Microbiology* 2005; **71(1)**, 270-275.

[6] M Ikram, J Hassan, A Raza, A Haider, S Naz, A Ul-Hamid, J Haider, I Shahzadi, U Qamar and S Ali. Photocatalytic and bactericidal properties and molecular docking analysis of TiO_2 nanoparticles conjugated with Zr for environmental remediation. *RSC Advances* 2020; **10,** 30007-30024.

[7] V Chandrakala, V Aruna and G Angajala. Review on metal nanoparticles as nanocarriers: Current challenges and perspectives in drug delivery systems. *Emergent Materials* 2022; **5**, 1593-1615.

[8] KY Kumar, MK Prashanth, OK Alduaij, TA Yousef, KM Abualnaja and MS Raghu. Mentha arvensis mediated green synthesis of platinum doped TiO_2 nanocomposite for enhanced anticancer and photocatalytic degradation activity: Insights from molecular docking and DFT studies. *Inorganic Chemistry Communications* 2021; **134**, 108987.

[9] G Leon-Gutierrez, JE Elste, C Cabello-Gutierrez, C Millan-Pacheco, MH Martinez-Gomez, R Mejia-Alvare, V Tiwari and A Mejia. A potent virucidal activity of functionalized TiO_2 nanoparticles adsorbed with flavonoids against SARS-CoV-2. *Applied Microbiology and Biotechnology* 2022; **106(18)**, 5987-6002.

[10] NA Mazurkova, YE Spitsyna, NV Shikina, ZR Ismagilov, SN Zagrebel'nyi and EI Ryabchikova. Interaction of titanium dioxide nanoparticles with influenza virus. *Nanotechnologies in Russia* 2010; **5**, 417-420.

[11] S Jafari, B Mahyad, H Hashemzadeh, S Janfaza, T Gholikhani and L Tayebi. Biomedical applications of TiO_2 nanostructures: Recent

advances. *International Journal of Nanomedicine* 2020; **15**, 3447-3470.

[12] Q Wang, JY Huang, HQ Li, AZJ Zhao, Y Wang, KQ Zhang, HT Sun and YK Lai. Recent advances on smart TiO_2 nanotube platforms for sustainable drug delivery applications. *International Journal of Nanomedicine* 2016; **2017(12)**, 151-165.

[13] RH Aguilera-del-Toro, F Aguilera-Granja and EE Vogel. Structural and electronic properties of $(TiO_2)_{10}$ clusters with impurities: A density functional theory investigation. *Journal of Physics and Chemistry of Solids* 2019; **135**, 109107.

[14] CA Lipinski, F Lombardo, BW Dominy and PJ Feeney. Experimental and computational approaches to estimate solubility and permeability in drug discovery and development settings. *Advanced Drug Delivery Reviews* 1997; **23(1-3)**, 3-25.

[15] M Frisch, G Trucks, HB Schlegel, GE Scuseria, M Robb, JR Cheeseman, G Scalmani, V Barone, GA Petersson, H Nakatsuji, X Li, M Caricato, A Marenich, J Bloino, B Janesko, R Gomperts, B MENNUCCI, H Hratchian, JV Ortiz, A izmaylov, ..., DJ Fox. *Gaussian 16, revision A.03*. Gaussian, Inc., Wallingford, 2016.

[16] AD Becke. Density-functional exchange-energy approximation with correct asymptotic behavior. *Physical Review A* 1988; **38**, 3098.

[17] C Lee, W Yang and RG Parr. Development of the Colle-Salvetti correlation-energy formula into a functional of the electron density. *Physical Review B* 1988; **37**, 785.

[18] PJ Hay and WR Wadt. Ab initio effective core potentials for molecular calculations. Potentials for the transition metal atoms Sc to Hg. *The Journal of Chemical Physics* 1985; **82(1)**, 270-283.

[19] R Dennington, TA Keith and JM Millam. *GaussView, version 6.0.16.* Semichem, Inc., Shawnee Mission, 2016.

[20] NM O'Boyle, AL Tenderholt and KM Langner. Cclib: A library for package-independent computational chemistry algorithms. *Journal of Computational Chemistry* 2008; **29(5)**, 839-845.

[21] ED Glendening, AE Reed, JE Carpenter and F Weinhold. *NBO 3.0 program manual.* CCL, Florida, 1990.

[22] T Lu and F Chen. Multiwfn: A multifunctional wavefunction analyzer. *Journal of Computational Chemistry* 2012; **33(5)**, 580-592.

[23] Z Jin, X Du, Y Xu, Y Deng, M Liu, Y Zhao, B Zhang, X Li, L Zhang, C Peng, Y Duan, J Yu, L Wang, K Yang, F Liu, R Jiang, X Yang, T You, X Liu, X Yang, ..., H Yang. Structure of Mpro from SARS-CoV-2 and discovery of its inhibitors. *Nature* 2020; **582(7811)**, 289-293.

[24] J Lan, J Ge, J Yu, S Shan, H Zhou, S Fan, Q Zhang, X Shi, Q Wang, L Zhang and X Wang. Structure of the SARS-CoV-2 spike receptor-binding domain bound to the ACE2 receptor. *Nature* 2020; **581(7807)**, 215-220.

[25] PW Rose, A Prlic, A Altunkaya, C Bi, AR Bradley, CH Christie, LD Costanzo, JM Duarte, S Dutta, Z Feng, RK Green, DS Goodsell, B Hudson, T Kalro, R Lowe, E Peisach, C Randle, AS Rose, C Shao, YP Tao, ..., SK Burley. The RCSB protein data bank: Integrative view of protein, gene and 3D structural information. *Nucleic Acids Research* 2017; **45(1)**, 271-281.

[26] A Douangamath, D Fearon, P Gehrtz, T Krojer, P Lukacik, CD Owen, E Resnick, C Strain-Damerell, A Aimon, P Abranyi-Balogh, J Brandão-Neto, A Carbery, G Davison, A Dias, TD Downes, L Dunnett, M Fairhead, JD Firth, SP Jones, A Keeley, GM Keserü, ..., MA Walsh. Crystallographic and electrophilic fragment screening of the SARS-CoV-2 main protease. *Nature Communications* 2020; **11**, 5047.

[27] J Medina-Barandica, N Contreras-Puentes, A Taron-Dunoyer, M Duran-Lengua, A Alviz-Amador. *In-silico* study for the identification of potential destabilizers between the spike protein of SARS-CoV-2 and human ACE-2. *Informatics in Medicine Unlocked* 2023; **40**, 101278.

[28] A Waterhouse, M Bertoni, S Bienert, G Studer, G Tauriello, R Gumienny, FT Heer, TAP de Beer, C Rempfer, L Bordoli, R Lepore and T Schwede. SWISS-MODEL: Homology modelling of protein structures and complexes. *Nucleic Acids Research* 2018; **46(1)**, 296-303.

[29] GM Morris, R Huey, W Lindstrom, MF Sanner, RK Belew, DS Goodsell and AJ Olson.

AutoDock4 and AutoDockTools4: Automated docking with selective receptor flexibility. *Journal of Computational Chemistry* 2009; **30(16)**, 2785-2791.

[30] Dassault Systèmes. *Discovery studio modeling environment*. Dassault Systèmes, France, 2017.

[31] R Maharjan, K Gyawali, A Acharya, M Khanal, MP Ghimire and TR Lamichhane. Artemisinin derivatives as potential drug candidates against *Mycobacterium tuberculosis*: Insights from molecular docking, MD simulations, PCA, MM/GBSA, and ADMET analysis. *Molecular Simulation* 2024; **50(11)**, 717-728.

[32] A Acharya, M Khanal, R Maharjan, K Gyawali, BR Luitel, R Adhikari, DD Mulmi, TR Lamichhane and HP Lamichhane. Quantum chemical calculations on calcium oxalate and dolichin A and their binding efficacy to lactoferrin: An *in silico* study using DFT, molecular docking, and molecular dynamics simulations. *AIMS Biophys.* 2024; **11(2)**, 142-165.

[33] A Daina, O Michielin and V Zoete. SwissADME: A free web tool to evaluate pharmacokinetics, drug-likeness and medicinal chemistry friendliness of small molecules. *Scientific Reports* 2017; **7,** 42717.

[34] P Banerjee, AO Eckert, AK Schrey and R Preissner. ProTox-II: A webserver for the prediction of toxicity of chemicals. *Nucleic Acids Research* 2018; **46**, 257-263.

[35] R Meyer and AW Hauser. Geometry optimization using Gaussian process regression in internal coordinate systems. *Journal of Chemical Physics* 2020; **152**, 084112.

[36] O Noureddine, N Issaoui and OD Al-Dossary. DFT and molecular docking study of chloroquine derivatives as antiviral to coronavirus COVID-19. *Journal of King Saud University - Science* 2021; **33(1)**, 101248.

[37] N Issaoui, H Ghalla, S Muthu, H Flakus and B Oujia. Molecular structure, vibrational spectra, AIM, HOMO–LUMO, NBO, UV, first order hyperpolarizability, analysis of 3-thiophenecarboxylic acid monomer and dimer by Hartree–Fock and density functional theory. *Spectrochim. Spectrochimica Acta Part A: Molecular and Biomolecular Spectroscopy* 2015**;** **136**, 1227-1242.

[38] B Borah and TG Devi. Characterization of Zn (L-Proline) 2 complex using spectroscopic techniques and DFT analysis. *Journal of Molecular Structure* 2020; **1210**, 128022.

[39] E Barim and F Akman. Synthesis, characterization and spectroscopic investigation of *N*-(2-acetylbenzofuran-3-yl) acrylamide monomer: Molecular structure, HOMO–LUMO study, TD-DFT and MEP analysis. *Journal of Molecular Structure* 2019; **1195**, 506-513.

[40] P Chattaraj, S Nath and B Maiti. Reactivity descriptors. *Computer-Aided Drug Design and Drug Discovery* 2003; **11**, 295.

[41] RG Pearson. Absolute electronegativity and hardness: Applications to organic chemistry. *The Journal of Organic Chemistry* 1989; **54(6)**, 1423-1430.

[42] N GF, V Vetrivelan and M Prasath. Enhancing therapeutic efficacy and safety profile of Favipiravir through noble metal loaded silica nanocomposites: A quantum chemical and molecular docking study for COVID-19 treatment. *Journal of Organometallic Chemistry* 2024; **1017**, 123291.

[43] T Koopmans. Über die Zuordnung von Wellenfunktionen und Eigenwerten zu den einzelnen Elektronen eines Atoms. *Physica* 1934; **1(1-6)**, 104-113.

[44] GF Nivetha, V Vetrivelan, S Muthu and M Prasath. Adsorption behavior, different green solvent effect and surface enhanced Raman spectra (SERS) investigation on inhibition of SARS-CoV-2 by antineoplastic drug Carmofur with silver/gold/platinum loaded silica nanocomposites: A combined computational analysis and molecular modelling approach. *Results in Chemistry* 2023; **6**, 101096.

[45] M Miar, A Shiroudi, K Pourshamsian, AR Oliaey and F Hatamjafari. Theoretical investigations on the HOMO–LUMO gap and global reactivity descriptor studies, natural bond orbital, and nucleus-independent chemical shifts analyses of 3-phenylbenzo [d] thiazole-2 (3 H)-imine and its para-substituted derivatives: Solvent and substituent effects. *Journal of*

Chemical Research 2021; **45**, 147-158.

[46] P Sjoberg, JS Murray, T Brinck, P Politzer. Average local ionization energies on the molecular surfaces of aromatic systems as guides to chemical reactivity. *Canadian Journal of Chemistry* 1990; **68(8)**, 1440-1443.

[47] E Scrocco and J Tomasi. *Advances in quantum chemistry.* E. Hoggan - Institut Pascal, France, 1978.

[48] R Abel, T Young, R Farid, BJ Berne and RA Friesner. Role of the active-site solvent in the thermodynamics of factor Xa ligand binding. *Journal of the American Chemical Society* 2008; **130(9)**, 2817-2831.

[49] H AlRabiah, S Muthu, F Al-Omary, AM Al-Tamimi, M Raja, RR Muhamed and AAR El-Emam. Molecular structure, vibrational spectra, NBO, Fukui function, HOMO-LUMO analysis and molecular docking study of 6-[(2-methylphenyl) sulfanyl]-5 propylpyrimidine-2, 4 (1H, 3H)-dione. *Macedonian Journal of Chemistry and Chemical Engineering* 2017; **36(1)**, 59-80.

[50] C Cassidy, JM Halbout, W Donaldson and CL Tang. Nonlinear optical properties of urea. *Optics Communications* 1979; **29(2)**, 243-246.

[51] K Fukui. Role of frontier orbitals in chemical reactions. *Science* 1982; **218(4547)**, 747-754.

[52] RG Parr and W Yang. Density functional approach to the frontier-electron theory of chemical reactivity. *Journal of the American Chemical Society* 1984; **106(14)**, 4049-4050.

[53] M Vimala, SS Mary, R Ramalakshmi and S Muthu. Theoretical description of green solvents effect on electronic property and reactivity of Tert-butyl 4-formylpiperidine-1-carboxylate. *Computational and Theoretical Chemistry* 2021; **1201**, 113255.

[54] C Morell, A Grand and A Toro-Labbe. New dual descriptor for chemical reactivity. *The Journal of Physical Chemistry A* 2005; **109(1)**, 205-212.

[55] M Kurt, PC Babu, N Sundaraganesan, M Cinar and M Karabacak. Molecular structure, vibrational, UV and NBO analysis of 4-chloro-7-nitrobenzofurazan by DFT calculations. *Spectrochimica Acta Part A: Molecular and Biomolecular Spectroscopy* 2011; **79(5)**, 1162-1170.

[56] ME Lestard, DM Gil, O Estevez-Hernandez, MF Erben and J Duque. Structural, vibrational and electronic characterization of 1-benzyl-3-furoyl-1-phenylthiourea: An experimental and theoretical study. *New Journal of Chemistry* 2015; **39(9)**, 7459-7471.

[57] F Weinhold and CR Landis. *Valency and bonding:* A natural bond orbital donor-acceptor perspective. *Cambridge University Press, Cambridge,* 2005.

[58] C James, AA Raj, R Reghunathan, V Jayakumar and IH Joe. Structural conformation and vibrational spectroscopic studies of 2,6-bis(p-N,N-dimethyl benzylidene) cyclohexanone using density functional theory. *Journal of Raman Spectroscopy* 2006; **37(12)**, 1381-1392.

[59] ER Johnson, S Keinan, P Mori-Sanchez, J Contreras-Garcia, AJ Cohen and W Yang. Revealing noncovalent interactions. *Journal of the American Chemical Society* 2010; **132(18)**, 6498-6506.

[60] RA Boto, JP Piquemal and J Contreras-Garcia. Revealing strong interactions with the reduced density gradient: A benchmark for covalent, ionic and charge-shift bonds. *Theoretical Chemistry Accounts* 2017; **136(139)**, 1-9.

[61] F Giordanetto, C Tyrchan and J Ulander. Intramolecular hydrogen bond expectations in medicinal chemistry. *ACS Medicinal Chemistry Letters* 2017; **8(2)**, 139-142.

[62] I Rozas, I Alkorta and J Elguero. Behavior of ylides containing N, O and C atoms as hydrogen bond acceptors. *Journal of the American Chemical Society* 2000; **122(45)**, 11154-11161.

[63] X Wang, J Lan, J Ge, J Yu and S Shan. Crystal structure of SARS-CoV-2 spike receptor binding domain bound with ACE2. *Protein Data Bank* 2020. https://doi.org/10.2210/pdb6M0J/pdb

[64] M Khanal, A Acharya, R Maharjan, K Gyawali, R Adhikari, DD Mulmi, TR Lamichhane and HP Lamichhane. Identification of potent inhibitors of HDAC2 from herbal products for the treatment of colon cancer: Molecular docking, molecular dynamics simulation, MM/GBSA calculations, DFT studies, and pharmacokinetic analysis. *PLOS One* 2024; **19(7)**, 0307501.

[65] K Gyawali, R Maharjan, A Acharya, M Khanal, MP Ghimire and TR Lamichhane. Identification of catechin as main protease inhibitor of SARS-CoV-2 Omicron variant using molecular docking, molecular dynamics, PCA, DCCM, MM/GBSA and ADMET profiling. *Natural Product Research* 2024; **2**, 1-8.

[66] A Ali, GJ Mir, A Ayaz, I Maqbool, SB Ahmad, S Mushtaq, A Khan, TM Mir and MU Rehman. *In silico* analysis and molecular docking studies of natural compounds of Withania somnifera against bovine NLRP9. *Journal of Molecular Modeling* 2023; **29**, 171.